Engineering Structures 297 (2023) 116992

Contents lists available at ScienceDirect

Engineering Structures

journal homepage: www.elsevier.com/locate/engstruct

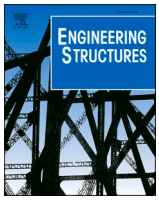

Bayesian-based prediction and real-time updating of axial deformation in high-rise buildings during construction

Yun Zhou [a], Xianming Luo [b,*], Peng Ye [b], Wenjie Zhang [b], Liaohui Qin [c], Zong Du [d]

[a] Professor, Key Laboratory for Damage Diagnosis of Engineering Structures of Hunan Province, Key Laboratory of Building Safety and Energy Efficiency of the Ministry of Education, College of Civil Engineering, Hunan University, Changsha 410082, China
[b] College of Civil Engineering, Hunan University, Changsha 410082, China
[c] Changsha Planning & Design Institute Co., Ltd, Changsha 410000, China
[d] China Construction Third Bureau First Engineering Co. Ltd, Wuhan 430040, China

ARTICLE INFO

Keywords:
Bayesian updating
Axial deformation
High-rise building
Vertical members
Creep and shrinkage

ABSTRACT

Estimating the axial deformation of concrete vertical members in a structure is challenging due to the shrinkage and creep characteristics of concrete together with the uncertainties involved in the construction process. To address the resulting inaccuracies, this paper presents a novel method that employs Bayesian theory to enhance the predicted results by incorporating measured strain from vertical members and equations for time-varying properties of concrete. The following five uncertain parameters are considered: environmental humidity, concrete strength, load transfer, concrete shrinkage calculation errors, and creep equation errors. The proposed method was experimentally evaluated on a twin tower high-rise building, with results showing that even with limited measured strain information, the uncertainty of the predicted results was significantly reduced and the predicted values were aligned closely with the measured values. The study also analyzed the impact of vertical deformation on the elevation deviation of adjacent wall-column members and the connected parts of the two towers.

1. Introduction

Since the 1950 s, a significant amount of research has been conducted on the shrinkage and creep characteristics of concrete materials, leading to the development of various prediction models such as the BP (Bazant & Panula) model [1], the modified BP models [2,3], the B3 model [4], the B4 model [5], and the GL2000 model [6]. Some design specifications, such as ACI 209R-92 [7] and MC 2010 [8], also prescribe the time-dependent properties of concrete materials. Accurate predicting of these properties is crucial in optimizing design and construction strategies, ensuring the durability and safety of concrete structures throughout their entire service life. Accurate prediction of axial deformations is crucial for effective structural design and analysis during the construction of tall structures, as the time-dependent properties of concrete play a significant role in these deformations. This is crucial as brittle partitions such as glass curtain walls, elevator shafts, or other areas can only accommodate a limited amount of vertical deformation [9]. Excessive axial deformation may cause elevator malfunctions, deformation or damage to pipelines, local cracking, and other abnormal functions [10,11]. Effectively addressing the supplementary deformations resulting from the time-dependent characteristics of concrete materials poses a notable challenge during the design phase, particularly when dealing with tall structures characterized by prolonged construction durations and substantial vertical dimensions [12,13]. Also, since the load conditions of vertical members during the construction stage are complex, it is essential to address in advance how to reasonably consider and eliminate the influence of additional deformation during the construction process.

To address this issue, studies have been conducted on the effects of concrete shrinkage or creep characteristics on structural deformation. Zou et al. [14] conducted a one-year shrinkage and creep test on RC shear walls and found that under the same surface-to-volume ratio, the codes or proposed models underestimated the vertical deformation of RC shear walls. Wang et al. [15] predicted the axial deformation of a vertical member of a super-tall building using the modified B3 model and considering the distribution of structural component humidity. The traditional B3 model would overestimate the axial deformation of giant

* Corresponding author.
E-mail addresses: zhouyun05@hnu.edu.cn (Y. Zhou), luoxianming@hnu.edu.cn (X. Luo), ye0607@hnu.edu.cn (P. Ye), zhangwj29@hnu.edu.cn (W. Zhang), QLH12031203@163.com (L. Qin), carzy_2727@qq.com (Z. Du).

https://doi.org/10.1016/j.engstruct.2023.116992
Received 28 June 2023; Received in revised form 13 September 2023; Accepted 29 September 2023

Nomenclature

The following symbols are used in this paper:

A_c	cross sectional area of specimen;
c_1	normalization constant that ensures the posterior probability=1;
E_{ci}	elasticity modulus of concrete;
E_s	elasticity modulus of reinforcement;
f_{X_m}	probability density function of the parameters;
P_i	predicted value;
p_n	likelihood of n sampling;
s_{X_m}	standard deviation of the observed values;
t_0	load time from the concrete pouring;
$t_{0,adj}$	adjusted age at loading according to temperature;
t_s	concrete age at the beginning of drying;
f_{cm}	compressive strength of concrete at the age of 28 days;
J	creep function;
J_s	creep function considering reinforcement ratio;
$J_{si,j}$	strain induced by the load applied at time j on the structure at time i;
u	perimeter of the member in contact with the atmosphere.;
RH	relative humidity of the environment;
h	nominal size of the member;
$S_{\theta^{post}}$	variance of the random variable's posterior distribution;
X_i	measured value of time i;
$\mathbf{X}$	observed result;
$\mathbf{X}_m$	observed result of time t_m;
X_m^n	calculated result corresponding to m time n sampling;
$\alpha_{bs}, \alpha_{ds1}, \alpha_{ds2}$	influence factor of cement type;
σ_c	constant load applied on the specimen;
σ_i	load induced by floor i;
ε_i	total strain at time i;
ε_c	strain of concrete;
ε_{cn}	strain that is independent of the load;
ε_{cc}	creep strain;
ε_{cs}	shrinkage strain;
ε_{cbs}	basic shrinkage strain;
ε_{cds}	drying shrinkage strain;
ε_{shi}	shrinkage strain at time i;
ρ	reinforcement ratio;
φ	creep coefficient;
φ_{bc}	basic creep coefficient;
φ_{dc}	drying creep coefficient;
$\theta_1, \theta_2, \theta_3, \theta_4, \theta_5$	Parameters for shrinkage, creep, humidity, concrete strength, and load uncertainty;
$\boldsymbol{\theta}^n$	uncertain parameters of n sampling;
$\overline{\boldsymbol{\theta}}^{post}$	mean of the random variable's posterior distribution.

vertical members if the humidity distribution is not considered. Baker et al. [16] considered the axial deformation of the Burj Khalifa tower during the design stage and verified that the existing calculation models and methods for predicting vertical displacement of super-tall structures were feasible. Zou et al. [17] predicted the axial deformation of vertical members in a super high-rise building using the shrinkage and creep equations provided by the MC 2010 and found that the error was relatively large during the early stage of concrete pouring, but gradually decreased as curing progressed. Similarly, Gao et al. [12] predicted the strain of a vertical member in a 335 m super high-rise structure in Wuhan, China and found that MC 2010 underestimated the shrinkage and creep of concrete. Zhao et al. [18] combined the B3 model with the fiber model to propose a method for predicting the section strain of a giant member and verified the model on a super high-rise structure. Tahmasebinia et al. [19] analyzed the overall vertical deformation of the Sydney Opera House and the damage to the prestressed cable in the concrete shell under shrinkage and creep effects. Xia et al. [20] monitored and analyzed the stress changes of several main components of the Guangzhou Tower in China during the construction phase. Since high-strength-low-shrinkage concrete was used in the project, the concrete shrinkage strain was only about 50% and the creep was only about 40% of the predicted value according to the ACI 209 code. By fitting a polynomial and calibrating its coefficients to the vertical deformation pattern of the entire structure, Blanc et al. [21] considered the complex axial deformation caused by creep during the construction process. Moragaspitiya et al. [22] proposed a method of updating the axial deformation of vertical members during the construction by establishing the relationship between the structural vibration characteristics and the axial deformation.

The time-dependent properties of concrete are influenced by numerous codes and exhibit significant variability. There is a large deviation in predicted results between various codes and calculation models [23,24]. Especially the range of test data is limited, and most experiments were performed under controlled environmental conditions [25,26]. Consequently, laboratory experiments are insufficient to address the impact of concrete's time-dependent properties on structural deformations during construction. To reduce this limitation, scholars have proposed probability theory and big data analysis methods to develop more accurate predictions of concrete's shrinkage and creep properties.

Madsen et al. [27] introduced the random model uncertainty factor to characterize the incompleteness and insufficiency of deterministic equations based on the BP model. Similarly, Li et al. [28] used the BP model to simulate concrete shrinkage and creep in a RC structure under stochastic loads and simplified the time-varying reliability problem in the stochastic process into a time-independent reliability problem for prediction. Bazant et al. [29] firstly predicted concrete shrinkage and creep using the Bayesian and numerical integration methods, but this method is only applicable to two or three input parameters and the creep effects are limited as linear changes with parameters. Bazant et al. [30,31] extended the prediction method for shrinkage and creep of concrete using sampling methods and used it to estimate the long-term deflection of a prestressed concrete segmented box girder bridge. Ojdrovic et al. [32] used a similar approach to significantly reduce the prediction error by introducing preliminary experimental data. Yang [33,34] also used Bayesian theory and early measured data to reduce the uncertainty of shrinkage and creep effects and analyzed the influence of input coefficients on creep effects. Han et al. [35] used importance sampling to ensure that the sampled data fall within the observed data range as much as possible to improve the prediction accuracy. Keitel et al. [24] used a sensitivity analysis method to compare the uncertainty of the creep prediction models GL2000, MC 2010, ACI 209, and B3, and found significant differences in the creep prediction results of different models. Gandomi et al. [36] proposed a new multi-objective genetic planning algorithm to establish a creep model suitable for a wide range of structural characteristics. Jin et al. [37] proposed a short-term creep test-based prediction method, introduced various creep models, and combined them to provide more reliable predictions of long-term creep behavior.

The practical application of time-dependent properties equations for concrete in construction projects was challenged by the issue of inadequate prediction accuracy. This is due to the lack of specific information regarding concrete materials during the design phase, as well as the uncertainties associated with the equations and construction site conditions. To address these issues, a super-tall twin-tower structure in Changsha was selected to evaluate the axial deformation of vertical

members under gravity load during the construction phase. Bayesian theory was used to incorporate the MC 2010 equation and other uncertain parameters as prior uncertain parameters. The strain sensor embedded in the structural members was utilized to update the posterior estimation results of vertical member strains, enabling real-time prediction, and updating of axial deformation of vertical members. Furthermore, the cumulative vertical displacement caused by the axial deformation on the column/wall and the connected structure was also calculated and analyzed to facilitate compensation for the height of vertical members during the construction process.

2. Time-dependent axial deformation calculation methods

During the construction process of a structure, a serious consideration of the axial deformation of vertical members is crucial due to its critical role in managing the cumulative vertical displacement resulting from the escalating gravity loads. Since each vertical member has its unique properties, including cross-sectional dimensions, reinforcement information, load-bearing capacity, the axial deformation of each member is quite different. In this paper, a specific calculation method for the axial deformation estimation of the vertical members in super high-rise structures is been proposed. This methodology accounts for the time-dependent axial compressive behavior of concrete vertical members under incrementally escalating gravity loads, as well as the selection of computational parameters. By accurately assessing the axial deformation, construction teams can compensate for the height of vertical members during the construction process.

2.1. Shrinkage and creep model

In accordance with the MC 2010 code [8], the shrinkage can be categorized into two distinct types: basic shrinkage $\varepsilon_{cbs}(t)$, which occurs even if no moisture loss, and drying shrinkage $\varepsilon_{cds}(t,t_s)$, which occurs as an additional consequence of moisture loss. Similarly, creep can be classified as either basic creep or drying creep. Furthermore, the code provides an equation for calculating the deformation of members under variable loads based on the superposition principle. Therefore, considering the changes in axial forces of the vertical members during the actual construction process of high-rise structures, this study evaluated the time-dependent behavior of concrete using the equation introduced by MC2010.

The equation for determining the shrinkage strain of a member at time t is expressed as follows:

$$\varepsilon_{cs}(t,t_s)=\varepsilon_{cbs}(t)+\varepsilon_{cds}(t,t_s) \tag{1}$$

where t_s represents the concrete age at the beginning of drying in days.

$$\varepsilon_{cbs}(t)=-\alpha_{bs}\left(\frac{0.1\cdot f_{cm}}{6+0.1\cdot f_{cm}}\right)^{2.5}\cdot 10^{-6}\cdot\left(1-\exp\left(-0.2\cdot\sqrt{t}\right)\right) \tag{2}$$

$$\varepsilon_{cds}(t,t_s)=\varepsilon_{cds0}(f_{cm})\cdot\beta_{RH}(RH)\cdot\beta_{ds}(t-t_s) \tag{3}$$

$$\varepsilon_{cds0}(f_{cm})=[(220+110\cdot\alpha_{ds1})\cdot\exp(-\alpha_{ds2}\cdot f_{cm})]\cdot 10^{-6} \tag{4}$$

$$\beta_{RH}=\begin{cases}-1.55\cdot\left[1-\left(\frac{RH}{100}\right)^3\right] & 40\le RH<99\%\cdot\left(\frac{35}{f_{cm}}\right)^{0.1}\\ 0.25 & RH\ge 99\%\cdot\left(\frac{35}{f_{cm}}\right)^{0.1}\end{cases} \tag{5}$$

$$\beta_{ds}(t-t_s)=\left(\frac{(t-t_s)}{0.035\cdot h^2+(t-t_s)}\right)^{0.5} \tag{6}$$

where f_{cm} is the average compressive strength of concrete at the age of 28 days; RH is the relative humidity of the environment; For 42.5 R cement, α_{bs}=600, α_{ds1}=6, andα_{ds2} = 0.012; $h=2A_c/u$ represents the nominal size of the member; A_c is the cross-sectional area of the member and u is the perimeter of the member in contact with the atmosphere.

The creep strain of a member can be calculated at time t using the equation:

$$\varepsilon_{cc}(t,t_0)=\frac{\sigma_c(t_0)}{E_{ci}}\varphi(t,t_0) \tag{7}$$

where E_{ci} is the modulus of elasticity at 28 days of age and $\sigma_c(t_0)$ is a constant load applied on the member at time t_0. The creep coefficient $\varphi(t,t_0)$ can be obtained using:

$$\varphi(t,t_0)=\varphi_{bc}(t,t_0)+\varphi_{dc}(t,t_0) \tag{8}$$

where $\varphi_{bc}(t,t_0)$ is the basic creep coefficient and $\varphi_{dc}(t,t_0)$ is the drying creep coefficient.

$$\varphi_{bc}(t,t_0)=\frac{1.8}{(f_{cm})^{0.7}}\cdot\ln\left(\left(\frac{30}{t_0}+0.035\right)^2\cdot(t-t_0)+1\right) \tag{9}$$

$$\varphi_{dc}(t,t_0)=\beta_{dc}(f_{cm})\cdot\beta(RH)\cdot\beta_{dc}(t_0)\cdot\beta_{dc}(t,t_0) \tag{10}$$

$$\beta_{dc}(f_{cm})=\frac{412}{(f_{cm})^{1.4}} \tag{11}$$

$$\beta(RH)=\frac{\left(1-\frac{RH}{100}\right)}{\sqrt[3]{0.1\cdot\frac{h}{100}}} \tag{12}$$

$$\beta_{dc}(t_0)=\frac{1}{0.1+t_0^{0.2}} \tag{13}$$

$$\beta_{dc}(t,t_0)=\left(\frac{(t-t_0)}{\beta_h+(t-t_0)}\right)^{\gamma(t_0)} \tag{14}$$

where $\beta_h=1.5\cdot h+250\cdot\left(\frac{35}{f_{cm}}\right)^{0.5}\le 1500\cdot\left(\frac{35}{f_{cm}}\right)^{0.5}$; $\gamma(t_0)=\frac{1}{2.3+3.5/\sqrt{t_{0,adj}}}$; $t_{0,adj}$ is the adjusted age at loading according to temperature.

To consider the actual construction process, the principle of superposition needs to be applied because the vertical members were subjected to gradually increased loads. This principle states that the total deformation of a structure under multiple load modes is equal to the sum of deformations caused by individual loads acting alone. Therefore, the total strain of a vertical member can be obtained by superimposing the strains during the construction process using Eqs. (1)-(14) under the constant load. This provides a more accurate prediction of the axial deformation of vertical members during construction.

$$\varepsilon_c(t)=\sigma_c(t_0)J(t,t_0)+\int_{t_0}^{t}J(t,\tau)\frac{\partial\sigma_c(\tau)}{\partial\tau}d\tau+\varepsilon_{cn}(t) \tag{15}$$

$$J(t,t_0)=\frac{1}{E_{ci}(t_0)}+\frac{\varphi(t,t_0)}{E_{ci}} \tag{16}$$

In Eq. (15) and (16), $J(t,t_0)$ is the creep function, representing the total stress-dependent strain per unit stress; $\varepsilon_{cn}(t)$ is the strain that is independent of the load and includes thermal and shrinkage strains; and $E_{ci}(t_0)$ is the elastic modulus of the concrete at time t_0.

2.2. Axial deformation in construction process

The deformation of vertical members in a structure comprises of two types of deformations, instantaneous and time dependent. Time-dependent deformation is mainly caused by creep and shrinkage effects. It is essential to calculate these deformations separately for each vertical member in each floor since they may have varying material and

geometric characteristics, as well as different environmental conditions. The calculation assumes that the vertical member is isotropic and only subjected to axial loads during the construction process. Therefore, the strain is assumed to be uniform along the vertical direction, and the total axial deformation can be obtained by multiplying the strain by the height of the member.

To simplify the computation process and consider the impact of reinforcement, it is assumed that the bond force between the reinforcement and concrete is negligible, and the loads are distributed proportionally based on the cross-section area of each material. Hence, Eq. (16) can be reformulated as:

$$J_s(t_i) = \frac{J(t_i)}{1 + \rho E_s / E_{ci}(t_i)} \tag{17}$$

In Eq. (17), ρ is the reinforcement ratio, and E_s represents the elastic modulus of the reinforcement.

During the construction process, the load acting on the vertical members varied with the concrete pouring time, requiring the division of deformation into n segments. It is assumed that the load during each time interval ($\sigma_1 \ldots \sigma_n$) remains constant. The strain of the vertical member at each moment can be calculated using Eq. (18). There is no external load ($\sigma_1 = 0$) during the first stage, and only shrinkage strain is generated.

$$\begin{Bmatrix} \varepsilon_1 \\ \varepsilon_2 \\ \varepsilon_3 \\ \varepsilon_4 \\ \cdots \\ \varepsilon_n \end{Bmatrix} - \begin{Bmatrix} \varepsilon_{sh1} \\ \varepsilon_{sh2} \\ \varepsilon_{sh3} \\ \varepsilon_{sh4} \\ \cdots \\ \varepsilon_{shn} \end{Bmatrix} = \begin{Bmatrix} J_{s1,1} & 0 & 0 & 0 & 0 & 0 \\ J_{s2,1} & J_{s2,2} & 0 & 0 & 0 & 0 \\ J_{s3,1} & J_{s3,2} & J_{s3,3} & 0 & 0 & 0 \\ J_{s4,1} & J_{s4,2} & J_{s4,3} & J_{s4,4} & 0 & 0 \\ \cdots & \cdots & \cdots & \cdots & \cdots & 0 \\ J_{sn,1} & J_{sn,2} & J_{sn,3} & J_{sn,4} & \cdots & J_{sn,n} \end{Bmatrix} \cdot \begin{Bmatrix} \sigma_1 \\ \sigma_2 \\ \sigma_3 \\ \sigma_4 \\ \cdots \\ \sigma_n \end{Bmatrix} \tag{18}$$

where ε_i is the total strain at time i, ε_{shi} is the shrinkage strain at time i, and J_{sij} represents the strain induced by the load applied at time j on the structure at time i.

For frame-core tube, the lateral resistance system of the structure mainly relies on the core tube shear wall, which means that the bending moment and shear force carried by the frame column can be neglected. The load transmitted by the upper storey σ_i is obtained by extracting the axial force from the design structural model, which consists of dead load and a construction load of 2.5kN/m^2 [38]. The creep and elastic deformation of a vertical member are closely related to the construction process (pouring time), while shrinkage is not related to it [39].

2.3. Uncertainty of axial deformation in vertical members

Concrete shrinkage and creep are affected by various factors such as material properties, environmental conditions, and loading conditions. The uncertainties associated with these factors may result in variations in the magnitude of shrinkage and creep. These uncertainties can be broadly categorized into internal, external, and measurement uncertainties [27,29,31]. Internal uncertainties arise due to the stochastic nature of physical mechanisms involved in creep and are relatively small, so they are generally ignored in structural design. External uncertainties arise due to errors in material parameters and environmental factors that influence those parameters, such as humidity. Measurement uncertainties generally result from errors in strain measurements and can be excluded from test data.

In this study, the external uncertainties associated with material properties and environmental conditions are considered. These uncertainties can significantly bias the prediction of shrinkage and creep in concrete structures, and therefore, their impact needs to be quantified and accounted for in structural design. It is imperative to acknowledge that the existing design equations in the code can potentially lead to considerable computational deviation [34]. This is due to the inherent degree of error that arises during the fitting process of the equations. Consequently, uncertain parameters θ_1 and θ_2 were introduced to account for the errors in the shrinkage and creep equation calculations, respectively. By directly multiplying the uncertain variables with the calculation expressions such as Eq. (19) and Eq. (20), the resulting uncertainty in this form of expression is more consistent with the discreteness of experimental data [27]. The prior mean values of θ_1 and θ_2 are 1, based on the statistical analysis by previous researchers [8], the variance of these uncertain parameters is determined to be 0.451 and 0.339, respectively.

Firstly, the primary environmental factor that affects concrete shrinkage and creep is humidity (*RH*). However, *RH* is often treated as a constant in calculation models. Therefore, to consider the meteorological conditions of the project location, *RH* is regarded as an uncertain parameter θ_3 with a mean of 70 and a variance of 20. Secondly, due to the inherent uncertainty of concrete material, the concrete strength is often inconsistent with the design value. Thus, the concrete strength is set as an uncertain parameter θ_4 with a mean of 60 and a variance of 20, based on the information obtained from the vertical members. Finally, the uncertainty in the load transmission in the structure is considered, where the axial load of each moment was multiplied by an uncertain parameter θ_5 (has a mean of 1, a variance of 0.5), as shown in Eq. (21). The axial load of the vertical member may vary up to 45%, depending on the consideration and analysis method [40,41]. To facilitate the calculation process, all uncertain parameters were assumed to follow a Gaussian distribution. The list of uncertain parameters about their meanings, prior means, and prior variances are all presented in Table 1.

$$\varepsilon_{cs}(t, t_s) = \theta_1 \cdot [\varepsilon_{cbs}(t) + \varepsilon_{cds}(t, t_s)] \tag{19}$$

$$\varepsilon_{cc}(t, t_0) = \theta_2 \cdot \left[\frac{\sigma_c(t_0)}{E_{ci}} \varphi(t, t_0) \right] \tag{20}$$

$$\sigma_{axi} = \theta_5 \cdot \sigma_i \tag{21}$$

3. Bayesian theory and updating methods

Bayesian theory provides an effective approach for dealing with uncertain events by treating uncertain parameters as probability distributions. In this way, pre-assumed uncertain parameter models can be used to analyze specific problems. By constructing the likelihood function and updating the observed results, the probability distribution of the uncertain parameters can be continually updated to make the predicted results more reliable.

The basic expression for predicting and updating using the Bayesian method is as follows:

$$P(\theta_1, \theta_2, \theta_3, \theta_4, \theta_5 | \mathbf{X}) = c_1 P(\mathbf{X} | \theta_1, \theta_2, \theta_3, \theta_4, \theta_5) \cdot P(\theta_1, \theta_2, \theta_3, \theta_4, \theta_5) \tag{22}$$

Table 1
Uncertain parameters.

Symbol	θ_1	θ_2	θ_3	θ_4	θ_5
Meaning	Shrinkage coefficient	Creep coefficient	Ambient humidity	Concrete strength	Load transfer coefficient
Prior Mean	1	1	70	60	1
Prior Variance.	0.451	0.339	20	20	0.5

where c_1 is a normalization constant that ensures the posterior probability is equal to 1; $\mathbf{X}$ denotes the observed result; $P(\theta_1,\theta_2,\theta_3,\theta_4,\theta_5|\mathbf{X})$ represents the posterior result, $P(\mathbf{X}|\theta_1,\theta_2,\theta_3,\theta_4,\theta_5)$ represents the likelihood function, and $P(\theta_1,\theta_2,\theta_3,\theta_4,\theta_5)$ is the prior information; The observed data at each time point t_m corresponds to a set of results $\mathbf{X}_m$. By using Latin hypercube sampling (LHS)[42] and prior information, m can be calculated from each set of sampled results using Eq. (18), resulting in n sets of sampled results X_m^n. Assuming that the five uncertain parameters are independent, the Naive Bayes approach is adopted. According to the Naive Bayes method, the likelihood function can be expressed as:

$$P\left(\boldsymbol{X}\middle|\theta_1^n,\theta_2^n,\theta_3^n,\theta_4^n,\theta_5^n\right)=\prod_{m=1}^{M}f_{X_m}(X|\boldsymbol{\theta}^n)=\prod_{m=1}^{M}\frac{1}{s_{X_m}\sqrt{2\pi}}\exp\left[-\frac{1}{2}\left(\frac{X_m-X_m^n}{s_{X_m}}\right)^2\right] \tag{23}$$

where f_{X_m} is the probability density function of the parameters, s_{X_m} is the standard deviation of the observed values; and X_m^n is the calculated result corresponding to certain time point in each sampling; The constant multiplication factor can be discarded since all the probabilities of the parameters are relative values. Therefore Eq. (22) can be expressed as:

$$P(\theta_1,\theta_2,\theta_3,\theta_4,\theta_5|\mathbf{X})=c\cdot\exp\left[-\frac{1}{2}\sum_{m=1}^{M}\left(\frac{X_m-X_m^n}{s_{X_m}}\right)^2\right]=c\cdot p_n \tag{24}$$

where the constant term c can also be eliminated since $\sum_n P(\boldsymbol{\theta}^n|\boldsymbol{X})=1$, thus $c=1/\sum_n P_n$; The updated parameters were obtained by multiplying the prior parameters with the corresponding likelihood term p_n. Since the posterior distribution also follows a Gaussian distribution, the mean and variance of the random variable's posterior distribution can be determined as follows:

$$\overline{\boldsymbol{\theta}}^{post}=\frac{1}{\sum_n p_n}\sum_n p_n\boldsymbol{\theta}^n \tag{25}$$

$$S_{\theta^{post}}=\sqrt{\frac{1}{\sum_n p_n}\sum_n p_n(\theta^n-\overline{\theta}^{post})^2} \tag{26}$$

The posterior distribution mean and variance of the structural response corresponding to $\boldsymbol{\theta}$ are:

$$\overline{X}_m^{post}=\frac{1}{\sum_n p_n}\sum_n p_n X_m^n \tag{27}$$

$$S_{X_m^{post}}=\sqrt{\frac{1}{\sum_n p_n}\sum_n p_n(X_m^n-\overline{X}_m^{post})^2} \tag{28}$$

By employing Bayesian inference, the sensor-instrumented members were updated and once the error reached a stable range, the updated parameters were utilized for predicting axial deformation of all the other vertical members. By continuously collecting strain data, an increasing amount of data becomes available for updates. As a result, the predicted results gradually converge towards a liable value. Utilizing the updated parameters, it becomes possible to further predict the axial compression deformation of vertical members, thereby compensating for the overall vertical deformation of the tower and enhancing construction quality. The process of Bayesian updating, and axial deformation prediction is depicted in Fig. 1.

4. Case study

4.1. Project overview

The project is based on a currently under-construction super high-rise twin-tower building (Shengtong-Meixi Lake international headquarters center) located in Changsha, China. The building comprises two buildings, Tower A and Tower B, with Tower A having a height of 279.65 m and consisting of 59 floors, while Tower B has 49 floors and is 219.65 m high. In Tower A, strengthening has been implemented on the 23rd, 34th, and 45th floors, with each level incorporating three sets of outrigger trusses to connect the frame columns and shear walls. The structure of both towers features a frame-core tube design, and the connection between them is a high-altitude steel structure corridor with rigid connections, spanning three floors between the 35th to 37th floors of Tower A and between the 44th to 46th floors of Tower B, at a height of 150 m. A schematic of the structure and a typical floor are shown in Fig. 2.

4.2. Strain gauge instrumentation

The vertical members located on the 1st floor of Tower B were cast in April 2021, whereas those of Tower A were cast in September 2021. In May 2022, a structural health monitoring system (Fig. 3(a)) was implemented when Tower A was constructed at the 16th floor. Therefore, the 17th floor of Tower A was firstly selected as a monitoring storey. The sensors are installed in three sets of wall and column members, as shown in Fig. 3. The basic information of the members is provided in Table 2. As the formwork was removed approximately 7 days after the concrete pouring, the initial strain changes of the concrete

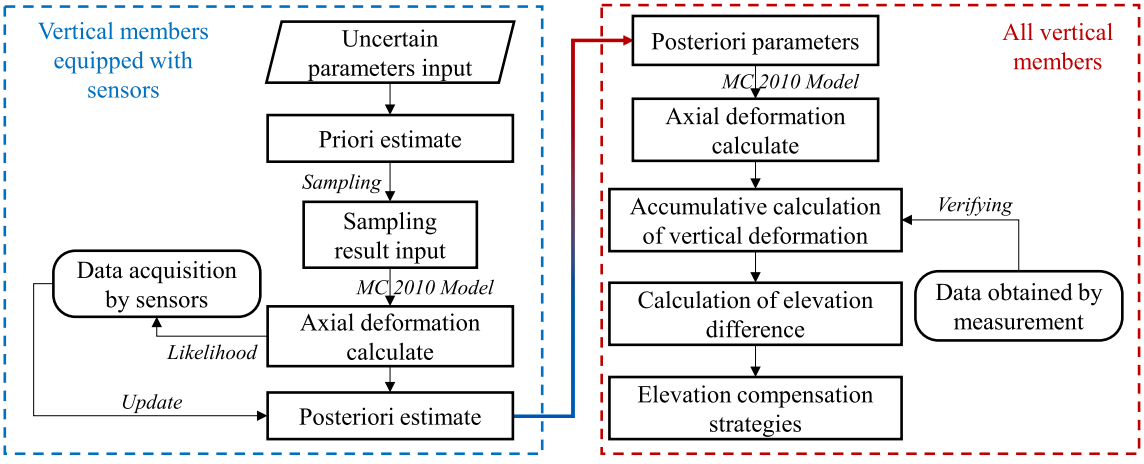

Fig. 1. Bayesian inference process for predicting axial deformation.

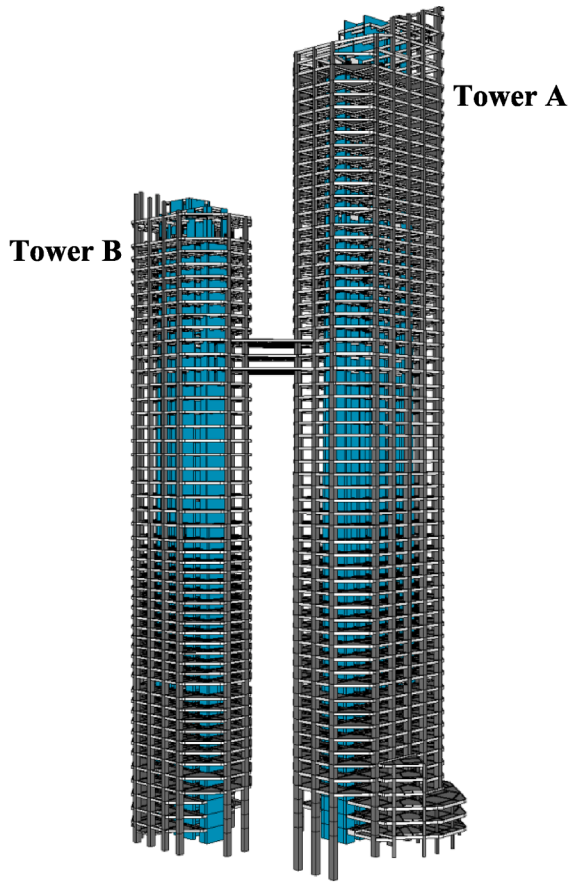

(a) Schematic of entire structure

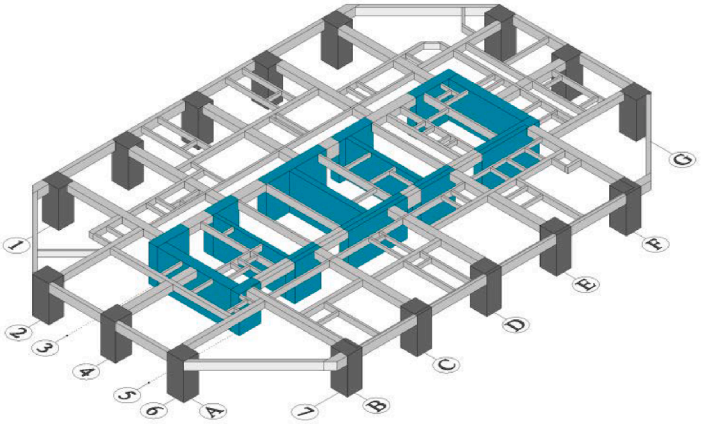

(b) Standard floor of Tower A

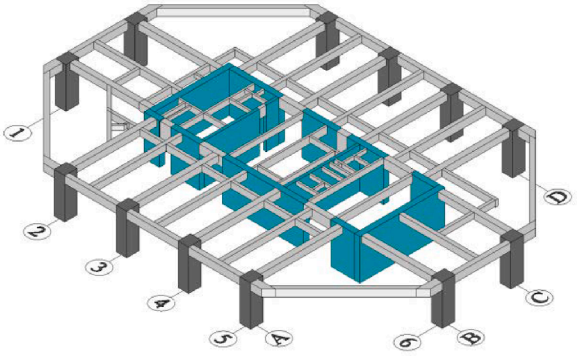

(c) Standard floor of Tower B

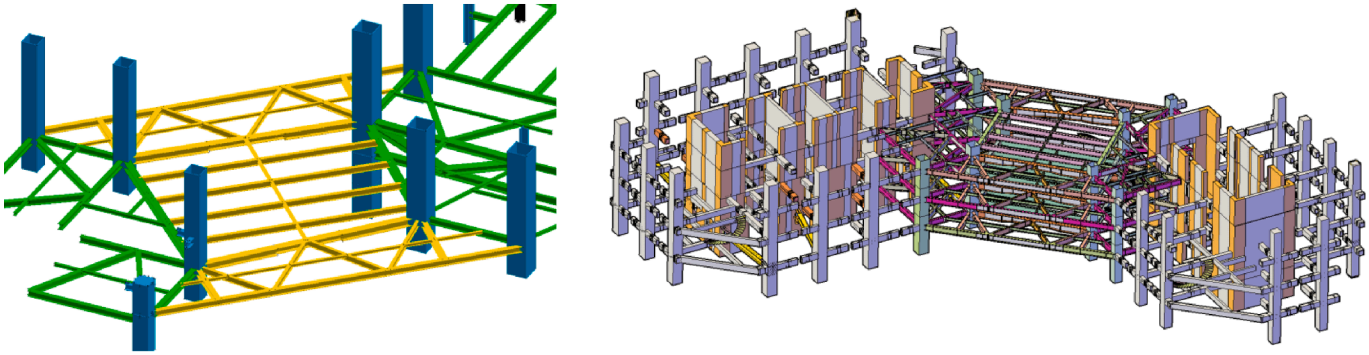

(d) Schematic diagram of corridor and corridor floor structure

(e) Visual representations of the project

(f) Current construction status

Fig. 2. SNTO Meixi Lake international headquarters center.

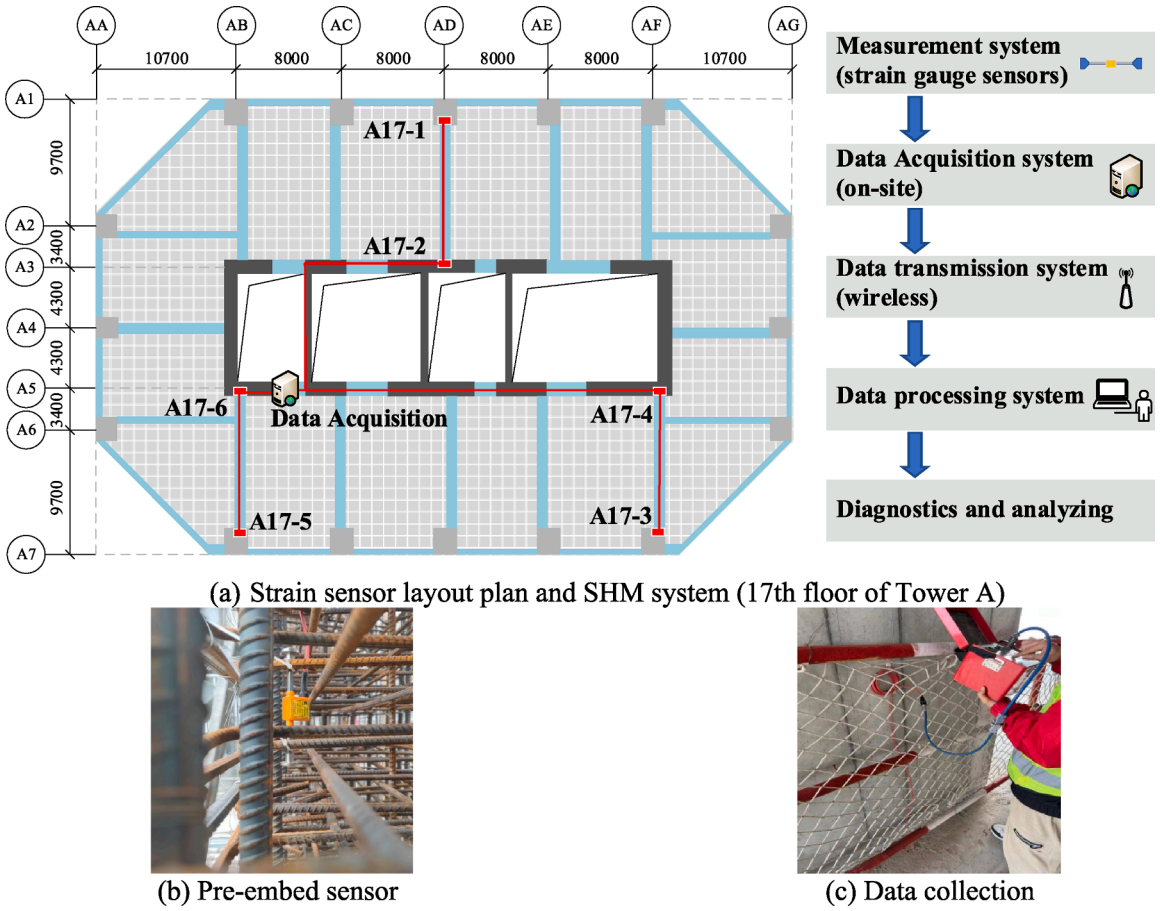

Fig. 3. Strain gauge instrumentation.

Table 2
Information of vertical members.

	A17-1	A17-2	A17-3	A17-4	A17-5	A17-6
Reinforcement ratio, %	0.95	0.91	0.95	0.91	0.95	0.91
nominal size *h*, mm	897	873	897	710	897	789
Height, mm	4100					
Concrete strength, MPa	60					
Type of cement	P II 52.5					

pouring were recorded manually.

4.3. Predicted results

Due to the time lags in the removal of formwork during the construction phase, all data were manually collected on-site at intervals of approximately 2 to 5 days. A cumulative period of 240 days was considered as the basis for calculations. The study employed LHS sampling to generate 50 sets of parameter data, calculated predictions, and updated results for axial deformations of concrete members using short-term measured data. The results are shown in Fig. 4 with (a)-(c) representing the updated results for the A17-1 sensor position frame column (A-D × A-1) considering 15%, 50%, and 100% of the collected data respectively. It can be observed that the prior estimation underestimates the vertical deformation, but with the data points updated, the posterior estimation interval gradually decreases, and the estimation results approach the actual deformation. Fig. 4 (d)-(f) represent the updated results of the A17-2 sensor location shear wall (A-D × A-3). The observation reveals that the prior parameter calculation tends to overestimate the actual deformation for shear wall members. However, as the number of considered test data points increases, this overestimation diminishes. Fig. 4 (g)-(l) shows the prediction process for the members at A17-3 (A-F × A-7) and A17-6 (A-B × A-5), which exhibit the same trend as A17-1 and A17-2.

Fig. 5 shows the prior and posterior distributions for the five uncertain parameters. It can be seen that after updating, the standard deviation of the parameters decreases. According to the posterior parameter results, the shrinkage calculation results of the frame column (A17-1, A17-3) are smaller than the measured deformation, while the creep calculation equation is slightly lower than the collected data. Therefore, the posterior calculation coefficients θ_1 and θ_2 for shrinkage and creep, respectively, are greater than 1. However, for the shear wall members (A17-2, A17-6), the shrinkage prediction in MC 2010 is slightly higher than the measured value, and the creep calculation result is slightly higher than the measured value. The prior and posterior results of the humidity θ_3 and concrete strength coefficients θ_4 remain almost consistent. But for the load transfer coefficient θ_5, the load condition used in the prior calculation is too large, indicating that the actual load is much smaller than the previously assumed load. Comparing the predicted and collected data, it is found that the vertical deformation of the shear wall is smaller than that of the frame column, which is consistent with previous research findings [13,43]. Although shear walls

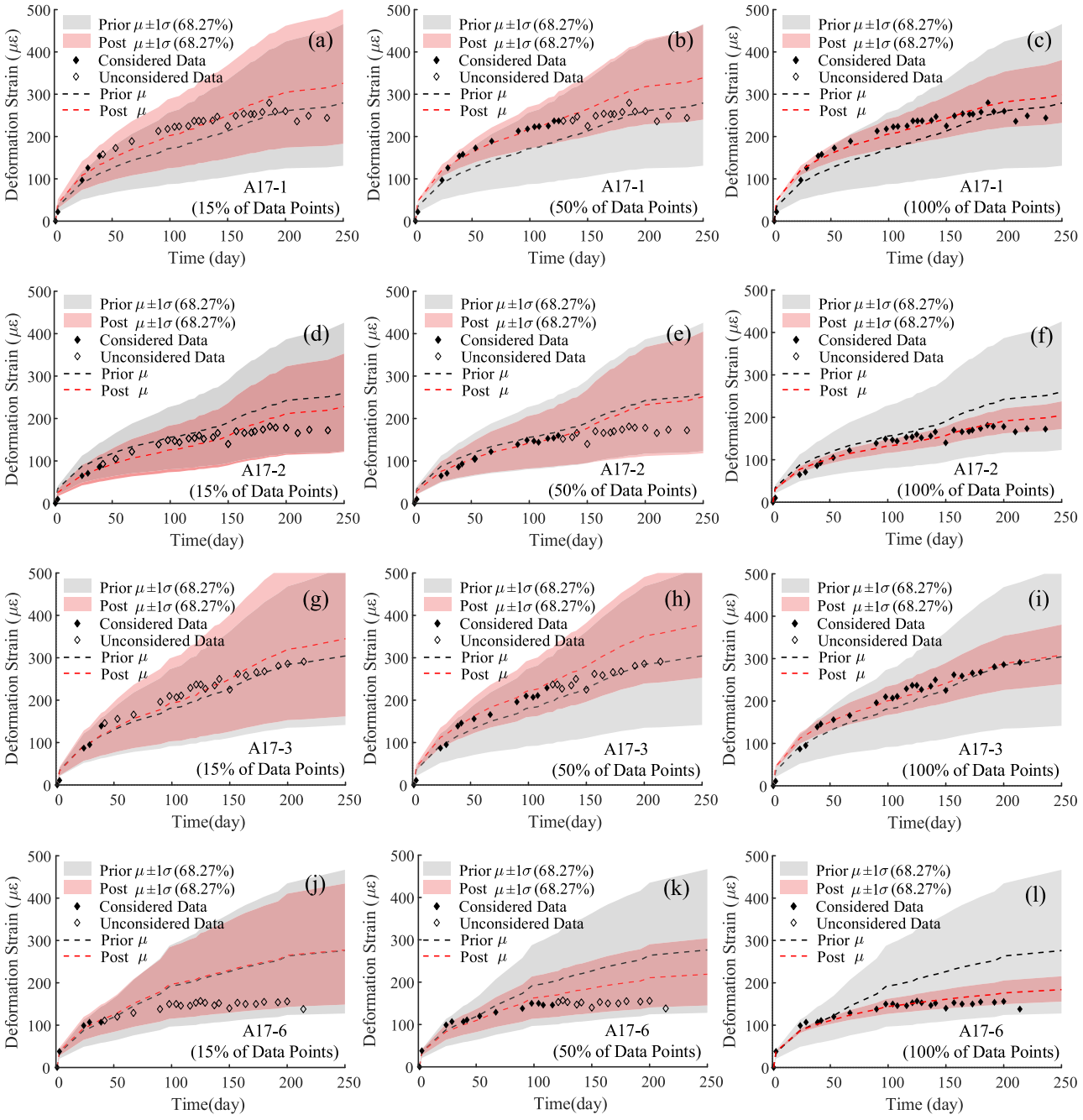

Fig. 4. Axial deformation strain prediction and results. (a)-(c): A17-1 column (A-D × A-1); (d)-(f): A17-2 wall (A-3 × A-D); (g)-(i): A17-3 column (A-F × A-7); (j)-(l): A17-6 wall (A-B × A-5).

sustain greater structural gravity loads, their larger cross-sectional areas result in lower axial stresses, therefore less deformation is related to the axial stress.

To assess the accuracy and rationality of the predicted results, mean square error (MSE) is used to evaluate the error between predicted and measured data as shown in Eq. (29).

$$MSE = \frac{1}{n}\sum_{i=1}^{n}(P_i - X_i)^2 \tag{29}$$

where n is the number of collected data points; P_i is the predicted value (in this study, the posterior mean of the parameter was taken as the predicted value), and X_i is the measured value.

The relationship between the prediction error and the number of considered data points is shown in Fig. 6. It can be observed that the prediction error decreases significantly with the increase of considered data points, and when the number of considered data points exceeds 10, the error remains within a constant range, indicating that the prediction results are within a credible range. Moreover, the comparison of prediction errors of vertical member reveal that, except for A17-6, the other members converged with relatively few observed data. Despite taking a longer time for A17-6 to converge, its computation error gradually approaches that of other members as the number of considered data points increase.

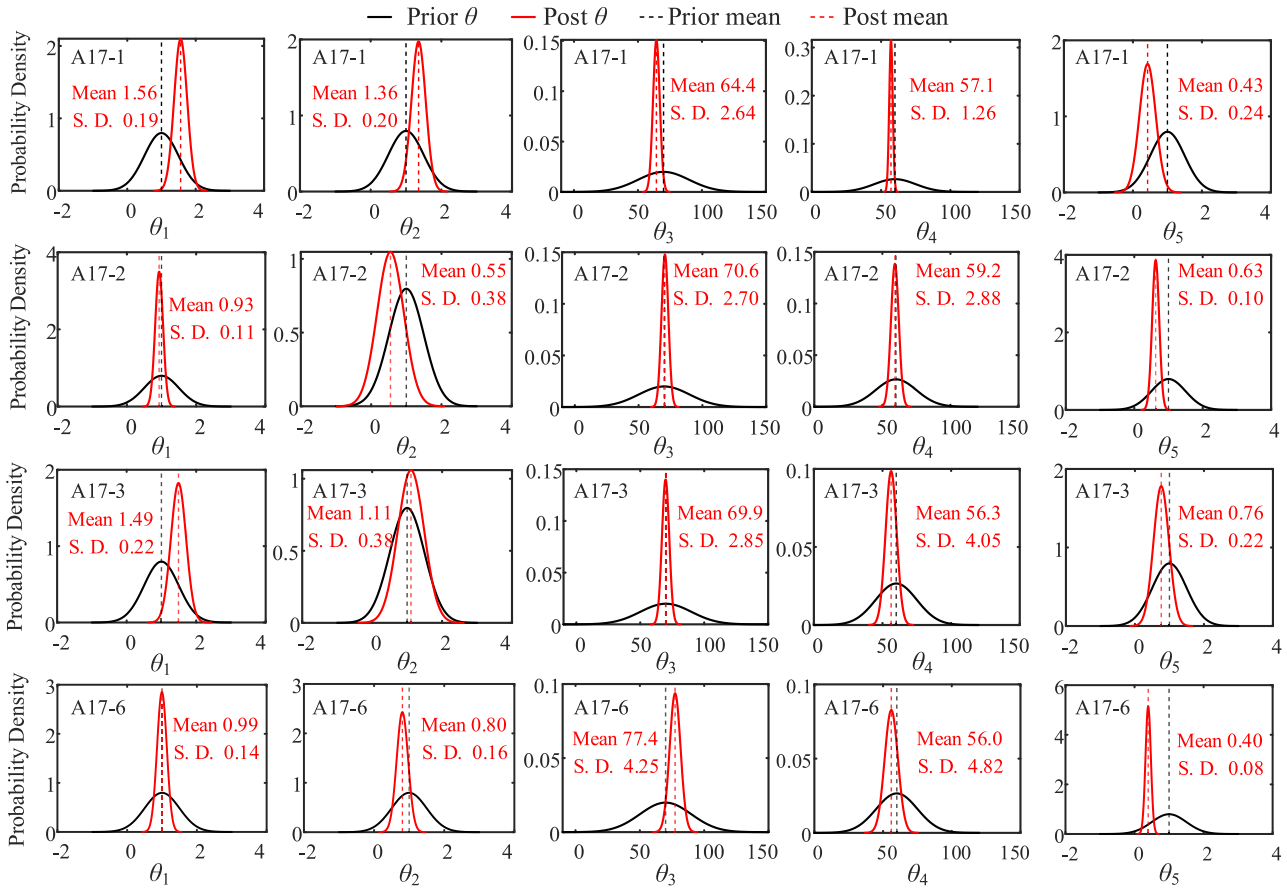

Fig. 5. Prior and posterior parameter distribution.

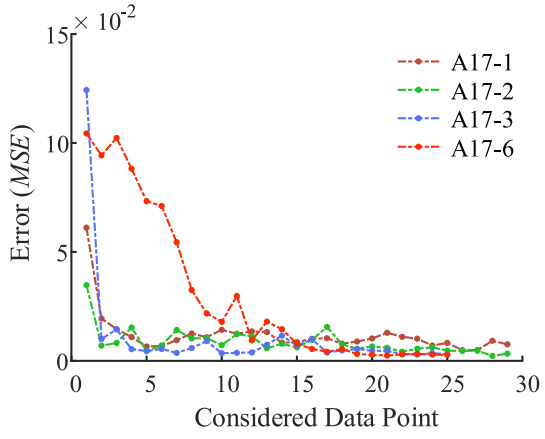

Fig. 6. Relationship between prediction error and considered data point.

Axial deformation calculations are also performed on the vertical members of other floors, as shown in Fig. 7, from which it can be concluded that the updated prediction results for the axial deformation of the vertical members are generally more accurate than those of the prior estimation. The deformation of the frame columns is generally larger than that of the shear walls, which is consistent with previous research findings. The estimation of axial deformation for the floors that have not yet been constructed is predicted based on a rate of 1 floor/15 days. It is important to indicate that the accuracy of these predictions could be affected by various factors such as changes in construction conditions, environmental factors, and material properties, which should be taken into consideration in further predictions.

5. Verification and calculation of vertical displacement

5.1. Verification of vertical displacement

To verify the cumulative effect of axial deformation of vertical members on the floor elevation, a leveling measurement was used to extend the 1-meter elevation line of each floor to the outside of the frame column. The vertical distance between each reflector was then observed using a total station, which was recorded as the measured vertical displacement, as shown in Fig. 8. In this project, the 1-meter elevation line of the 5th and 24th floors of Tower A were extended, and their vertical heights were measured at 426 days (construction up to the 30th floor) and 553 days (construction up to the 35th floor) after the first floor was cast. The recorded measurements showed a difference of 5 mm between the first observation result of 84.165 m and the second observation result of 84.160 m. The calculated overall vertical displacement of the floors at 426 days and 553 days are shown in Fig. 9 (a) and (b), where the vertical displacement of each floor is the sum of all axial deformations of the vertical members below it. The difference between △2 and △1 in the figure is 4.81 mm, which is almost identical to the measurement result of 5 mm, indicating that the calculation method is reasonable considering the system error during the measurement process.

5.2. Vertical displacement and compensation design

Considering that the floor elevation has not been compensated in this

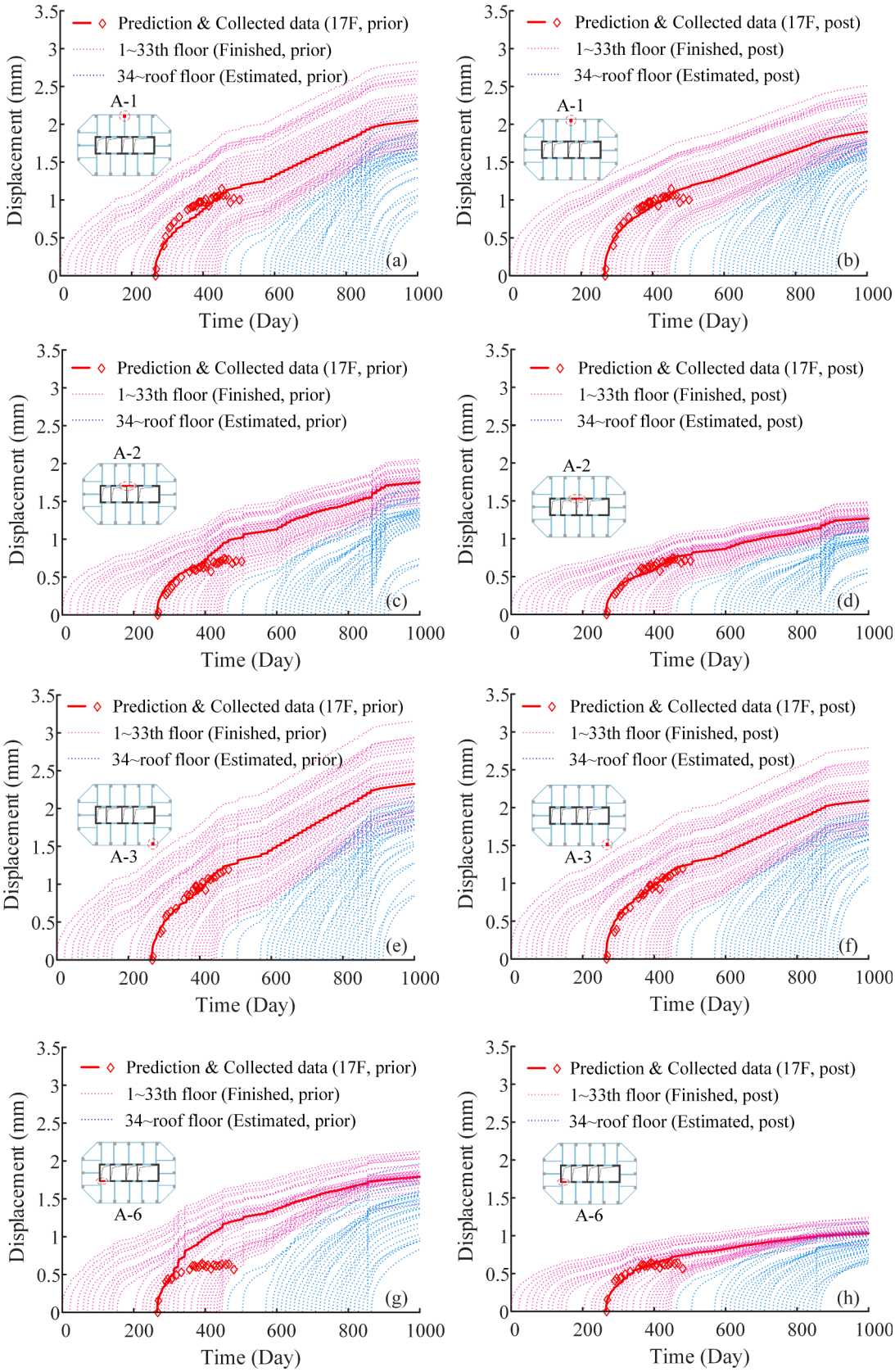

Fig. 7. Axial deformation development for each floor.

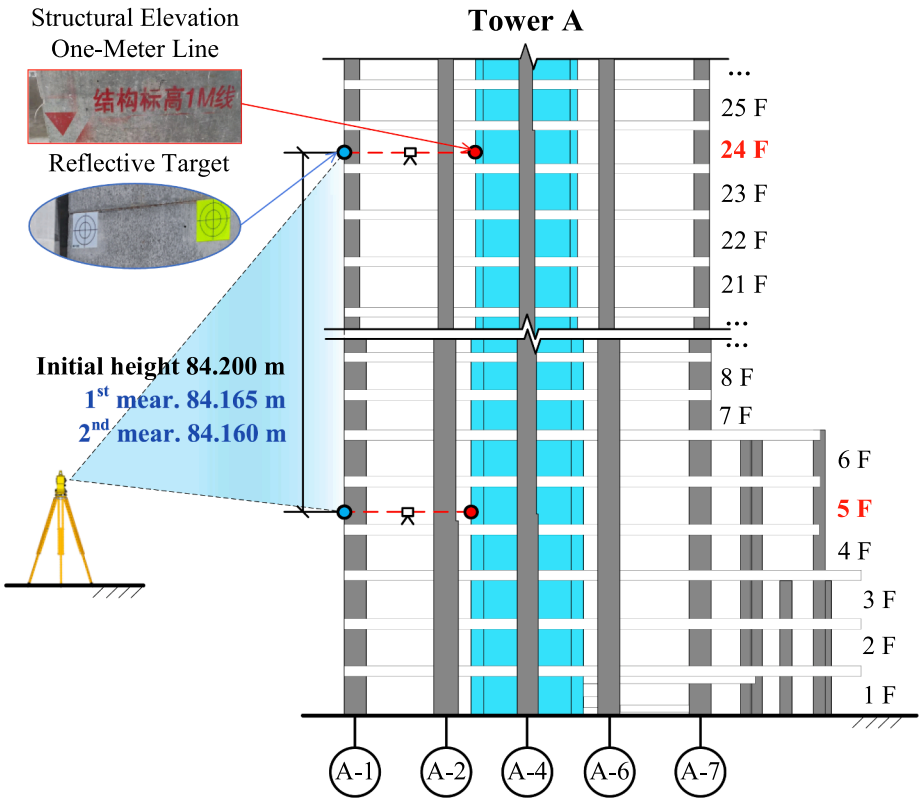

Fig. 8. Precision level measurement of vertical displacement.

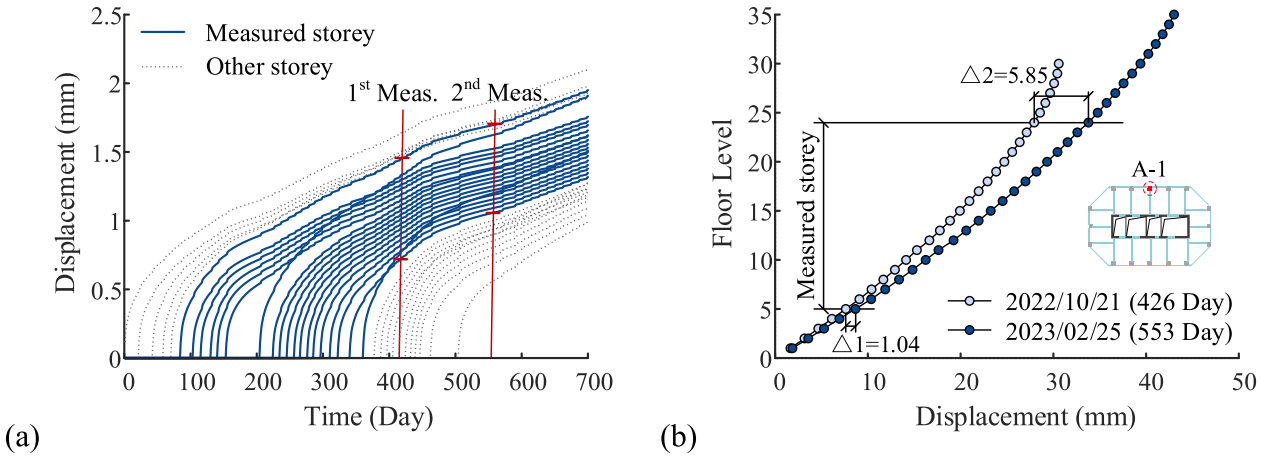

Fig. 9. Measurement range and measured results.

project, it can be concluded from the previous analysis that the deformation of the frame columns is greater than that of the shear walls, resulting in a certain deformation difference that will accumulate with the increase of height. Taking a group of vertical members (A17-1, A17-2) as an example, their vertical displacements at the position of the connecting layer and the top floor are shown in Fig. 10, where the deformation difference would reach 13.63 mm when Tower A construction reaches the connecting storey, and the accumulated deformation difference may reach 40.24 mm when the construction reached the top floor. This deformation difference may cause the horizontal connecting beam to tilt and generate a large bending moment at the beam end if the rigid boundary condition was designed, which may result in floor inclination and structural cracking. Therefore, it is necessary to compensate for the deformation of adjacent vertical members in advance to prevent such issues happens. Alternatively, in the absence of such conditions, the design requires the implementation of a specialized hinge-to-rigid connection transition joint.

Considering that the building features a double tower connected structure, with the connecting part located at a height of 150 m and the plan size and height of Tower A both greater than those of Tower B, the elevation of the connecting part is expected to be affected by non-uniform settlement and different axial deformations. Therefore, the vertical displacement of the vertical members in connecting storey is calculated, as shown in Fig. 11, which indicates that when Towers A and B were simultaneously constructed up to the level of the connecting floor, the vertical displacement difference at the connecting part is 4.36

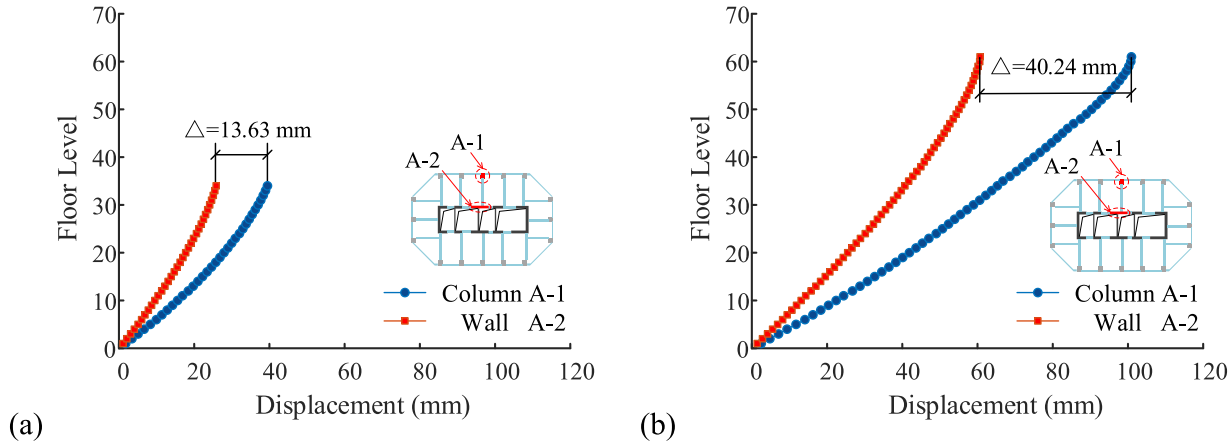

Fig. 10. Vertical displacement difference between adjacent columns and walls.

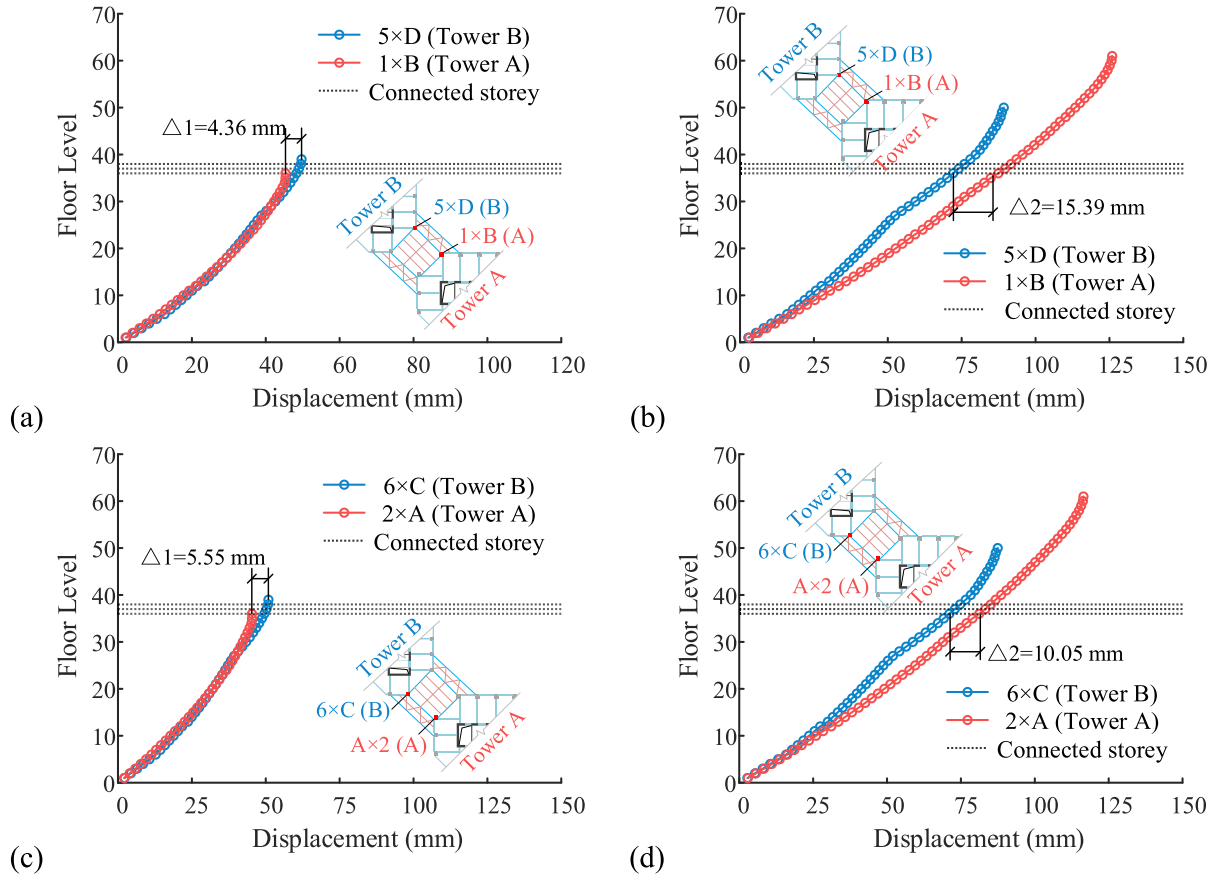

Fig. 11. Vertical displacement at the connected position.

mm, with Tower B showing greater deformation than Tower A. Based on the observed settlement, the bottom column settlement at this position isδ_A = 8 mm , δ_B = 8.8 mm, indicating that the elevation of the connecting part of Tower A is 5.16 mm higher than that of Tower B. This is because although the plan size of Tower A is larger than that of Tower B, the larger cross-section size of the vertical members in Tower A, due to its greater height, corresponds to a smaller axial compression ratio, resulting in smaller axial deformation than Tower B. However, as the construction progresses and Towers A and B are completed, the accumulated vertical displacement of Tower A is significantly larger than that of Tower B; meanwhile, the vertical displacement difference at the connecting position is 15.39 mm, with the elevation of the connecting position of Tower A being lower than that of Tower B. Fig. 11 (c)-(d) presents the cumulative vertical displacement at another connecting point, with a vertical cumulative displacement difference of 5.55 mm when both towers are constructed up to the connecting storey, and with bottom settlements ofδ_A = 8.3 mm, δ_B=7.7 mm. Therefore, at this stage, the elevation of the connection level for Tower A is 4.95 mm higher than that of Tower B. After both towers are topped out, the difference increased to 10.05 mm. Given that the minimum distance between the towers at the connecting part in this project is only 15.5 m and considering the development of settlement differences between the

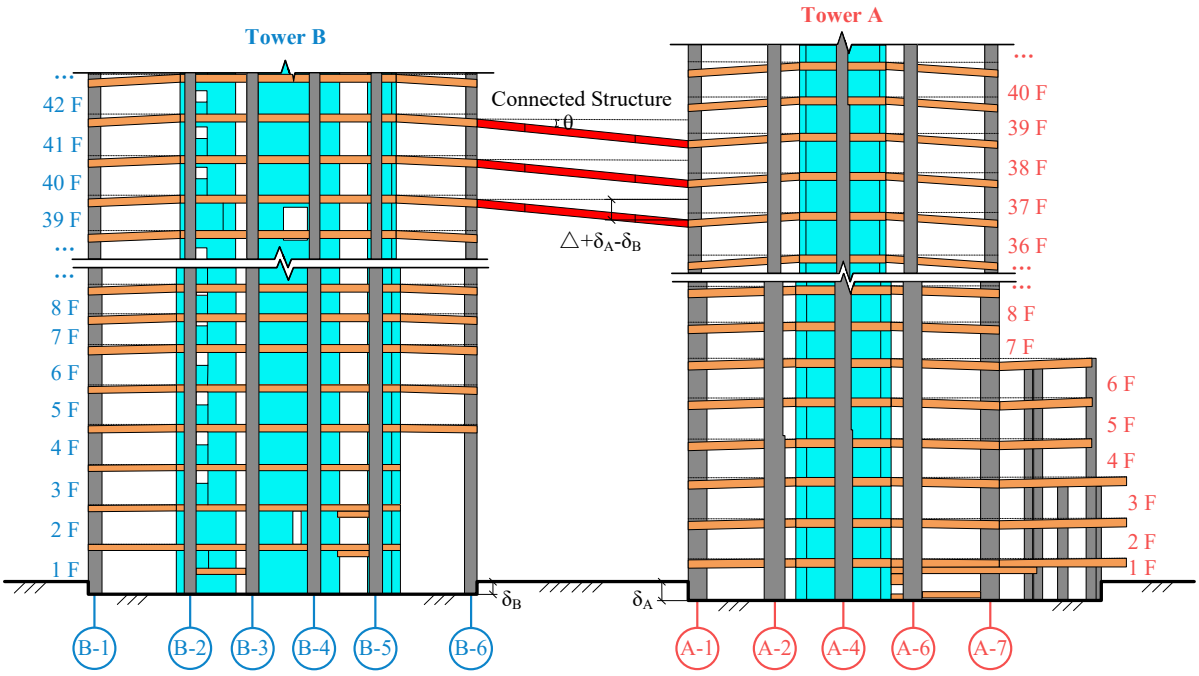

Fig. 12. Elevation difference at connected position.

towers, the inclination caused by the elevation difference at the connecting part may exceed 1/1000. Therefore, it is necessary to compensate for the cumulative vertical displacement of the two towers during construction to ensure the safety of the structure. See Fig. 12.

These findings suggest that the variation in elevation at the connected position is a time-dependent process that undergoes changes throughout the construction process. It is worth noting that the discrepancies in settlement contribute minimally to the overall elevation difference, as the latter is predominantly attributed to the cumulative axial deformation of vertical members. Furthermore, if the deformation difference of the vertical members is not compensated, it will have a certain impact on the structural members, regardless of whether it is the cumulative deformation difference of different vertical members within the tower or between connected positions of vertical members between towers.

6. Conclusions

A Bayesian-based method was proposed to predict the axial deformation of a super-tall twin tower structure, considering the time-dependent behavior of concrete. This approach utilizes the strain information from vertical members to estimate the elevation error caused by the overall vertical displacement of the building. To reduce prediction errors, actual deformations were measured on-site, ensuring a consistency between predicted and actual deformations. By incorporating a limited amount of measured data into the model, the accuracy of predictions was significantly improved, and a comprehensive understanding of the vertical displacement and its impact on the elevation accuracy was obtained. The following provides a summary of the study's achievements.

1. A method has been developed for predicting the axial deformation of vertical members during construction, considering changes in axial loads. This method is based on the MC 2010 equations for calculating concrete inelastic deformation. The calculation process assumes that axial loads remain constant within each time interval, based on the discrete construction schedule for each floor. The method accounts for shrinkage, creep, and elastic deformation during each time interval.
2. A Bayesian method was proposed to update the axial deformation prediction based on measured data. The uncertain parameters, including concrete strength, environmental humidity, calculation error, and load transfer error, were considered as Gaussian distributed variables. By using the measured data and the naive Bayes method to establish the likelihood function, the real-time prediction and updating of parameters were achieved.
3. As an example, several groups of wall-columns in a super high-rise twin-tower building under construction were embedded with strain sensors in the vertical structural components during the construction stage. The corresponding strain data was manually collected during the early stages of casting to obtain the development pattern of axial deformation throughout the construction process.
4. The entire construction process of the vertical members deformation was analyzed. The results were validated using surveying techniques, and the cumulative vertical displacement difference between different vertical members and the elevation difference of the connected positions between towers were calculated and analyzed. The calculation results can be used to guide the compensation of vertical displacement differences during the construction process and improve the safety of the structure.

CRediT authorship contribution statement

Yun Zhou: Funding acquisition, Resources, Conceptualization, Supervision, Writing – review & editing. **Xianming Luo:** Conceptualization, Methodology, Project administration, Formal analysis, Visualization, Validation, Writing – original draft. **Peng Ye:** Investigation, Validation. **Wenjie Zhang:** Investigation, Validation. **Liaohui Qin:** Validation. **Zong Du:** Resources, Supervision, Project administration.

Declaration of Competing Interest

The authors declare that they have no known competing financial interests or personal relationships that could have appeared to influence the work reported in this paper.

Data availability

Data will be made available on request.

Acknowledgements

The authors sincerely appreciate the funding support provided by the National Natural Science Foundation of China (NSFC) (No. 51878264, No. 52278306), the Science and Technology Progress and Innovation Project of the Department of Transportation of Hunan Province (201912), the Natural Science Foundation of Hunan Province of China (No. 2023JJ70003), and the Hydraulic Science and Technology Project of the Hunan Provincial Department of Water Resources (No. XSKJ2023059-31).

References

[1] Bazant ZP, Panula L. Practical prediction of time-dependent deformations of concrete. Mater Struct 1978;12(69):169–83.
[2] Bazant ZP, Kim JK, Panula L. Improved prediction model for time-dependent deformations of concrete: Part 1-Shrinkage. Mater Struct 1991;24:327–45.
[3] Bazant ZP, Kim JK. Improved prediction model for time-dependent deformations of concrete: Part 2-Basic creep. Mater Struct 1991;24:409–21.
[4] Bazant ZP, Murphy WP. Creep and shrinkage prediction model for analysis and design of concrete structures-model B3. Mater Struct 1995;28:357–65.
[5] R. Wendner, M.H. Hubler, Z.P. Bazant. The B4 Model for Multi-decade Creep and Shrinkage Prediction. *Ninth International Conference on Creep, Shrinkage, and Durability Mechanics (CONCREEP-9)*. MA, USA. 2013. https://doi.org/10.1061/9780784413111.051.
[6] Gardner NJ, Lockman MJ. Design provisions for drying shrinkage and creep of normal-strength concrete. ACI Mater J 2001;98(2):159–67. https://doi.org/10.14359/10199.
[7] ACI Committee 209. Prediction of Creep, Shrinkage, and Temperature Effects in Concrete Structures(209R-92). American Concrete Institute. 1992.
[8] CEB-FIP. Fib Model Code for Concrete Structures 2010. *International Federation for Structural Concrete (fib)*. 2010. https://doi.org/10.1002/9783433604090.
[9] Pan LB, Liu PC, Bakoss SL. Long-Term Shortening of Concrete Columns in Tall Buildings. J Struct Eng 1993;119(7):2258–62. https://doi.org/10.1061/(ASCE)0733-9445(1993)119:7(2258).
[10] Jayasinghe MTR, Jayasena WMVPK. Effects of Axial Shortening of Columns on Design and Construction of Tall Reinforced Concrete Buildings. Pract Period Struct Des Constr 2004;9(2):70–8. https://doi.org/10.1061/(ASCE)1084-0680(2004)9:2(70).
[11] Praveen M, David T, Nimal P, Chan T. A numerical method to quantify differential axial shortening in concrete buildings. Eng Struct 2010;32:2310–7. https://doi.org/10.1016/j.engstruct.2010.04.006.
[12] Gao F, Zhou H, Liang H, Weng S, Zhu H. Structural deformation monitoring and numerical simulation of a supertall building during construction stage. Eng Struct 2020;209:110033. https://doi.org/10.1016/j.engstruct.2019.110033.
[13] Elnimeiri MM, Joglekar MR. Influence of Column Shortening in Reinforced Concrete and Composite High-Rise Structures. ACI J 1989;SP 117–4:55–86. https://doi.org/10.14359/3318.
[14] Zou D, Liu T, Teng J, Du C, Li B. Influence of creep and drying shrinkage of reinforced concrete shear walls on the axial shortening of high-rise buildings. Constr Build Mater 2014;55:46–56. https://doi.org/10.1016/j.conbuildmat.2014.01.034.
[15] Wang L, Zhao X, Yan C. Time-dependent vertical shortening prediction for super-tall buildings by using a modified B3 model to consider moisture distribution. Eng Struct 2020;209:109994. https://doi.org/10.1016/j.engstruct.2019.109994.
[16] Baker WF, Korista DS, Novak LC, Pawlikowski J, Young B. Creep and Shrinkage and the Design of Supertall Buildings—A Case Study: The Burj Dubai Tower. ACI J 2007;SP 246–8:133–48. https://doi.org/10.14359/18983.
[17] Zou D, Du C, Liu T, Teng J, Cheng H. Time-dependent deformations of concrete columns under different construction load histories. Adv Struct Eng 2019;22(8):1845–54. https://doi.org/10.1177/1369433219828133.
[18] Zhao X, Wang L. Vertical shortening prediction for super-tall buildings considering enclosure effect and coupling effect. *The Structural Design of Tall and Special*. Buildings 2019;29(2). https://doi.org/10.1002/tal.1685.
[19] Tahmasebinia F, Fogerty D, Wu LO, Li Z, Sepasgozar SME, Zhang K, et al. Numerical Analysis of the Creep and Shrinkage Experienced in the Sydney Opera House and the Rise of Digital Twin as Future Monitoring Technology. Buildings 2019;137(9). https://doi.org/10.3390/buildings9060137.
[20] Xia Y, Ni YQ, Zhang P, Liao WY, Ko JM. Stress Development of a Supertall Structure during Construction: Field Monitoring and Numerical Analysis. Comput Aided Civ Inf Eng 2011;26:542–59. https://doi.org/10.1111/j.1467-8667.2010.00714.x.
[21] Blanc CM, Sanchez AO, Navarro IF. Analytical characterisation of axial shortening due to creep of reinforced concrete columns in tall buildings. Eng Struct 2021;228:111584. https://doi.org/10.1016/j.engstruct.2020.111584.
[22] Moragaspitiya HNP, Thambiratnam DP, Perera NJ, Chan THT. Development of a vibration-based method to update axial shortening of vertical load bearing elements in reinforced concrete buildings. Eng Struct. 2013;46:49–61. https://doi.org/10.1016/j.engstruct.2012.07.010.
[23] Goel R, Kumar R, Paul DK. Comparative Study of Various Creep and Shrinkage Prediction Models for Concrete. J Mater Civ Eng 2007;19(3):249–60. https://doi.org/10.1061/(ASCE)0899-1561(2007)19:3(249).
[24] Keitel H, Osburg AD. Uncertainty and sensitivity analysis of creep models for uncorrelated and correlated input parameters. Eng Struct 2010;32:3758–67. https://doi.org/10.1016/j.engstruct.2010.08.020.
[25] Hubler MH, Wendner R, Bazant ZP. Comprehensive Database for Concrete Creep and Shrinkage: Analysis and Recommendations for Testing and Recording. ACI Mater J 2015;112(4):547–58. https://doi.org/10.14359/51687453.
[26] Bazant ZP, Li GH. Unbiased Statistical Comparison of Creep and Shrinkage Prediction Models. ACI Mater J 2008;105(6):610–21. https://doi.org/10.14359/20203.
[27] Madsen HO, Bazant ZP. Uncertainty Analysis of Creep and Shrinkage Effects in Concrete Structures. ACI J 1983;80(13):116–27. https://doi.org/10.14359/10467.
[28] Li CQ, Melchers RE. Reliability Analysis of Creep and Shrinkage Effects. J. Struct. Eng. 1992;118(9):2323–37. https://doi.org/10.1061/(ASCE)0733-9445(1992)118:9(2323).
[29] Bazant ZP, Chern JC. Bayesian Statistical Prediction of Concrete Creep and Shrinkage. ACI J 1985;81(29):319–30. https://doi.org/10.14359/10686.
[30] Bazant ZP, Kim JK. Segmental Box Girder: Deflection Probability and Bayesian Updating. J Struct Eng 1988;115(10):2528–47. https://doi.org/10.1061/(ASCE)0733-9445(1989)115:10(2528).
[31] Bazant ZP, Liu KL. Random Creep and Shrinkage in Structures: Sampling. J Struct Eng 1985;111(5):1113–34. https://doi.org/10.1061/(ASCE)0733-9445(1985)111:5(1113).
[32] Ojdrovic RP, Zarghamee MS. Concrete Creep and Shrinkage Prediction from Short-Term Tests. ACI Mater. J. 1996;93(2):169–77. https://doi.org/10.14359/1416.
[33] Yang IH. Prediction of time-dependent effects in concrete structures using early measurement data. Eng Struct 2007;29:2701–10. https://doi.org/10.1016/j.engstruct.2007.01.015.
[34] Yang IH. Uncertainty and sensitivity analysis of time-dependent effects in concrete structures. Eng Struct 2007;29:1366–74. https://doi.org/10.1016/j.engstruct.2006.07.015.
[35] Han B, Xiang TY, Xie HB. A Bayesian inference framework for predicting the long-term deflection of concrete structures caused by creep and shrinkage. Eng Struct 2017;142:46–55. https://doi.org/10.1016/j.engstruct.2017.03.055.
[36] Gandomi AH, Sajedi S, Kiani B, Huang Q. Genetic programming for experimental big data mining: A case study on concrete creep formulation. Autom Constr 2016;70:89–97. https://doi.org/10.1016/j.autcon.2016.06.010.
[37] Jin SS, Cha SL, Jung HJ. Improvement of concrete creep prediction with probabilistic forecasting method under model uncertainty. Constr Build Mater 2018;184:617–33. https://doi.org/10.1016/j.conbuildmat.2018.06.238.
[38] Fan F, Wang HJ, Zhi XD, Huang G, Zhu EC, Wang H. Investigation of Construction Vertical Deformation and Pre-Deformation Control for Three Super High-Rise Buildings. Adv Struct Eng 2013;16(11):1885–97. https://doi.org/10.1260/1369-4332.16.11.1885.
[39] Fintel M, Khan FR. Effects of column creep and shrinkage in tall structures-analysis for differential shortening of columns and field observation of structures. ACI J 1969;66(12):957–67. https://doi.org/10.14359/7444.
[40] Samra RM. New Analysis for Creep Behavior in Concrete Columns. J Struct Eng 1993;121(3):399–407. https://doi.org/10.1061/(ASCE)0733-9445(1995)121:3(399).
[41] Kurc O, Lulec A. A comparative study on different analysis approaches for estimating the axial loads on columns and structural walls at tall buildings. Struct Design Tall Spec Build 2013;22:485–99. https://doi.org/10.1002/tal.699.
[42] Iman RL, Helton JC, Campbell JE. An approach to sensitivity analysis of computer models, Part I — Introduction, input variable selection and preliminary variable assessment. J Qual Technol 1981;3(13):174–83. https://doi.org/10.1080/00224065.1981.11978748.
[43] Sung WP, Se WC, Hyo SP. Moving average correction method for compensation of differential column shortenings in high-rise buildings. Struct Design Tall Spec Build 2013;22(9):718–28. https://doi.org/10.1002/tal.722.